Available online at www.sciencedirect.com
ScienceDirect
Journal of Nuclear Materials 356 (2006) 112–117
journal of nuclear materials
www.elsevier.com/locate/jnucmat

Irradiation-induced structural changes in martensitic steel T91

M. Grosse *, Y. Dai, S. Van Petegem

Paul Scherrer Institut, CH-5232 Villigen PSI, Switzerland

Abstract

The microstructure of T91 (9Cr1Mo) martensitic steels have been investigated with SANS and ASAXS techniques after irradiation in SINQ Target-3 with protons and neutrons. The SANS investigations cover specimens irradiated to doses between 3.9 and 9.8 dpa at temperatures $\leqslant$200 °C. The SANS intensities of the irradiated specimens show strong irradiation effects at $Q > 0.7$ nm^{-1}. The differences between the different irradiation states are weak. From the magnetic scattering contribution the size distributions of the irradiation induced defects were calculated. All size distributions were rather narrow with maxima at a diameter of about 0.8 nm. The ASAXS measurements were performed on reference and two samples irradiated to 9.1 and 9.7 dpa at 150 and 300 °C, respectively. The variation of the X-ray energy close to the Cr–K-absorption edge results in a contrast variation and shows information about chromium-containing inhomogeneities. At $Q > 0.7$ nm no irradiation-induced chromium effect could be detected. It indicates that the irradiation defects detected by SANS do not contain chromium. The chromium-containing inhomogeneities induced by irradiation are larger than the defects detected by SANS.

1. Introduction

Martensitic steels like T91 are candidates for the proton beam window materials of liquid metal spallation neutron sources like the MEGAPIE target or the targets of next generation spallation neutron sources. These windows are exposed to high radiation load. In order to understand the degradation of mechanical properties under irradiation the structural changes have to be investigated. The influence of chemical composition and thermo-mechanical treatment of the material as well as the influence of radiation parameters on type, amount and size of the radiation defects has to be studied to optimize the target window material to high radiation resistance.

The types of defects formed in martensitic steels during a combined proton and neutron irradiation are still under discussion. In [1] the defects formed after neutron irradiation in some martensitic steels, are interpreted as Cr-rich α′-precipitates. α′-precipitates were also found in [2] in ferritic steel but in martensitic steels γ-precipitates and dislocation loops were detected after proton irradiation. In [3] He-bubbles were found in F82H after proton irradiation. In [4] the development of He-bubbles after α-particle irradiation was studied.

* Corresponding author. Address: Forschungszentrum Karlsruhe, Hermann-von-Helmholz-Platz 1, 76344 Eggenstein-Leopoldshafen, Germany. Tel.: +49 7247 82 3884; fax: +49 7247 82 4567.
E-mail address: Mirco.Grosse@imf.fzk.de (M. Grosse).

0022-3115/$ - see front matter © 2006 Elsevier B.V. All rights reserved.
doi:10.1016/j.jnucmat.2006.05.026

In the present work, to obtain separate information about the different types of radiation defects, both small angle neutron (SANS) and anomalous small angle X-ray scattering (ASAXS) techniques were applied. As shown in [5] for radiation defects in ferritic steels the combination of these two complementary methods can provide sufficient information to prove the hypotheses about the type of these defects.

The contrast variation in the ASAXS experiment at X-ray energies close to the Cr-absorption edge gives the information about the Cr-rich α′-precipitates, but the distinction between He-bubbles, dislocation loops or nano-voids is impossible. The contrast difference between magnetic and nuclear SANS intensity gives additional information about the type of defects formed.

A description of the theoretical background is given in [5].

2. Material and measurements

2.1. Chemical composition and irradiation conditions

The investigations were performed on specimens irradiated in the SINQ spallation target (PSI, Villigen, Switzerland) in the framework of the STIP-1 irradiation programme. Table 1 gives the irradiation fluence and temperature of the specimens. Among them I01, I03 and I05 were used for the SANS measurements and I09 and I12 for the ASXAS analyses. In addition to the irradiated specimens, unirradiated samples were measured as the reference state. The chemical composition of the T91 martensitic steel is given in Table 2.

Table 1
Irradiation conditions of the specimens

Specimen	Fluence (dpa)	Irradiation temperature (°C)
I01	9.2–9.8	<220
I03	6.7–8.1	<220
I05	3.9–5.2	<220
I09	9.1	150
I12	9.7	300

Table 2
Chemical composition of the T91 specimens

Cr	Mo	Mn	V	Ni	Nb	C	Fe
8.32	0.86	0.48	0.20	0.06	0.06	0.09	Balance

2.2. SANS experiments

The SANS experiments were performed at the SANS-I facility at PSI with a wavelength of 0.47 nm in a magnetic field of 0.3 T. A special designed sample holder focuses the magnetic field lines to the sample and orients the field lines parallel in the sample. This setup corresponds with a conventional setup with a magnetic field strength of about 1.5 T. The beam cross section was $3 \times 3\ mm^2$. In order to handle the high activity of the samples a special sample chamber was constructed. The specimens were assembled into the sample holder in the hot cells of PSI and then transported to the SANS-experiment.

The SANS intensity was measured from sub-size 3PB-test specimens with a dimension of $2 \times 4 \times 20\ mm^3$. Due to fluence gradients along the major axis of the specimens, the measurements were performed at two positions, 5 mm from each end. Measurement time of 2 h per position was applied. The sample-to-detector distance was 1.6 m. Additional, measurements at distances of 6 and 18 m were performed to check whether there is any radiation effect at very low values of the scattering vector (Q).

2.3. ASAXS experiments

To prove the interpretation given in [1] that in martensitic steels an irradiation-enhanced separation of Fe-rich α and Cr-rich α′ phase occurs, ASAXS experiments were performed at the JUSIFA facility at HASYLAB (Hamburg). The SAXS patterns were measured with five X-ray energies at the lower energy side of the Cr–K-absorption edge. Table 3 gives the relevant scattering length parameters at the applied energies. Contrast variation effects can be expected for Cr-containing

Table 3
Real and imaginary part of the atomic form factor ($f+f'$, f'', respectively) of Cr and their mean values for T91, absorption coefficient μ and optimal thickness for the applied X-ray energies

	X-ray energy (eV)				
	5690	5900	5960	5980	5988
$f+f'$ (Cr)	21.5	20.0	18.7	17.6	15.3
f'' (Cr)	0.52	0.47	0.46	0.46	0.46
$f+f'$ (mean value[a] T91)	24.3	24.0	23.8	23.7	23.6
f'' (mean value[a] T91)	0.68	0.64	0.63	0.62	0.62
μ (T91)	708.5	640.6	622.8	616.9	614.8
Optimal thickness in μm	14.1	15.6	16.1	16.2	16.3

[a] For 91.68%Fe + 8.32%Cr.

inhomogeneities at the applied energies. The specimens I09 and I12 were measured together with an unirradiated reference specimen at sample-to-detector distances of 935 mm and 3635 mm. Measurement times of about 1 h per specimen and energy at the short distance and of more than 3.5 h for the long distance were applied.

3. Results and discussion

3.1. Results of the SANS measurements

Fig. 1 compares the magnetic SANS patterns measured at both positions of specimens I01, I03 and I05 with the patterns measured at the unirradiated state. The scattering measured at the unirradiated state can be described by a power law with an exponent of −4 and a constant scattering contribution. This constant contribution can be attributed to incoherent scattering of the different iron isotopes and monotonic Laue scattering produced by point defects and substitution atoms. The power law scattering indicates that only large inhomogeneities exist in the unirradiated material.

In Fig. 2 the constant scattering contributions are subtracted. After irradiation the small angle neutron scattering increases strongly at high Q values ($>0.7\ \mathrm{nm}^{-1}$). No significant differences are found between the specimens irradiated to the different fluences.

For the calculation of the size distribution of the radiation defects, the uncorrected data of Fig. 1 were used. The data was fitted using a log-normal size distribution of spherical shaped particles and a background contribution consisting of a sum of

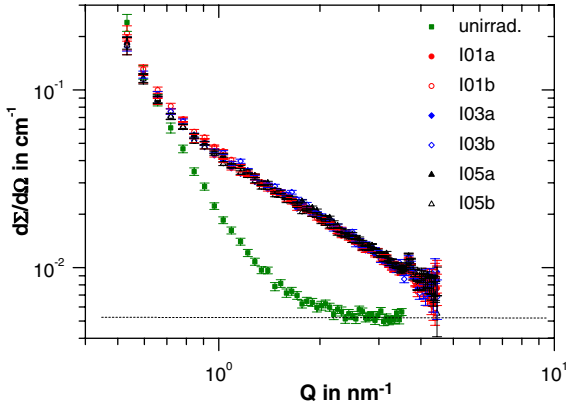

Fig. 1. SANS pattern of the unirradiated and the irradiated T91 samples.

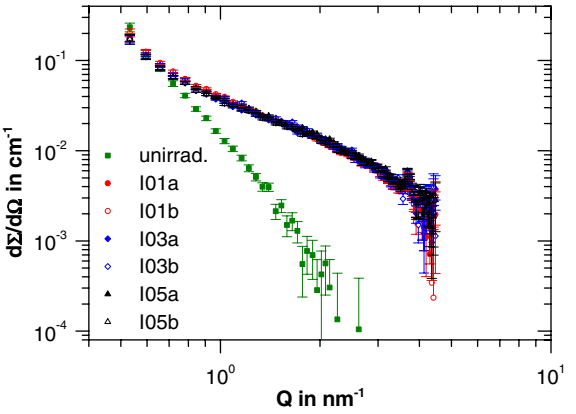

Fig. 2. SANS pattern corrected for constant background.

a power law and constant background. On the basis that the defects are para- or dia-magnetic, which is fulfilled for α′-precipitates, He-bubbles and nanovoids, no assumptions about composition and structure of these defects are necessary to determine their absolute volume fractions.

The results of this analysis are given in Fig. 3 and Table 4. As can be expected from the small differences in the SANS intensity, the size distribution curves of the different specimens are very similar. The maxima of the size distribution functions were determined at radii of about 0.4 nm. The volume fraction varies between 0.7 and 0.8 vol.%. The volume fractions of radiation defects for both positions of I05 specimen are unexpectedly high since the irradiation doses, helium concentrations and irradiation temperatures there were low. Nevertheless, it can be deduced from the results that the formation of radiation defects is in saturation because the volume fraction of the defects does not clearly depend on fluence.

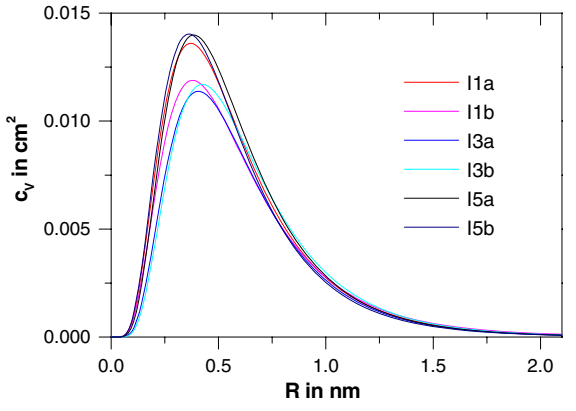

Fig. 3. Size distribution function of the radiation defects.

Table 4
Analysis results of the SANS data (a and b are the different measurement positions at the sample)

Specimen	Volume fraction c of the irradiation defects (vol.%)	Maximum of the size distribution function R_{max} (nm)
I1a	0.82	0.37
I1b	0.75	0.33
I3a	0.7	0.41
I3b	0.74	0.42
I5a	0.83	0.38
5b	0.81	0.36

Information about the possible composition of the precipitates can be obtained from the ratio between magnetic and nuclear SANS. In the literature the so-called A-parameter often used, which is the ratio of the scattering intensities measured perpendicular and parallel to the magnetization direction. Due to the magnetic scattering depends on the angle α between the scattering vector and the magnetization direction with $I_{mag} \sim \sin^2(\alpha)$ a separation of both scattering contributions is possible. It can also be calculated for a given structure from the differences between the scattering densities of the matrix and the inhomogeneities $\Delta\eta$ for magnetic and nuclear scattering, respectively,

$$A = \frac{I_\perp}{I_\parallel} = \frac{\Delta\eta^2_{mag} + \Delta\eta^2_{nuc}}{\Delta\eta^2_{nuc}}. \quad (1)$$

A detailed description of the theoretical background is given in [5].

The A-ratios determined from the experimental data do not depend on Q. They increase from 1.4 in the unirradiated state to values of about 2.0 after irradiation. It is in the range of the value measured in [1] (1.8 ± 0.3) and the value calculated for Cr reach α' precipitates (2.09–2.13) [1]. The A-ratio of pure Cr precipitates of 2.02 also agrees with the measured values.

3.2. Results of the ASAXS measurements

Fig. 4 shows the SAXS pattern of the two irradiated and the unirradiated states measured at the X-ray energy of 5988 eV. At this energy the strongest Cr effect of contrast variation should be expected. Only small differences were found. The data are corrected for constant scattering contributions (see further for more details about these corrections).

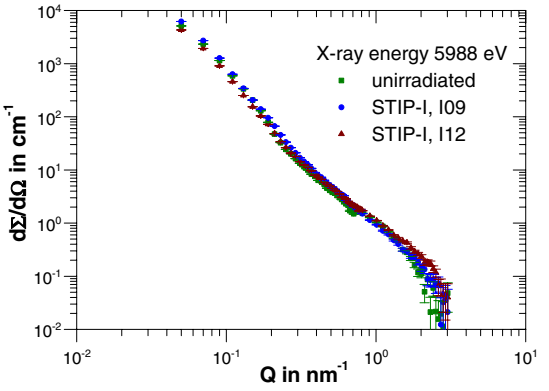

Fig. 4. SAXS patterns of the unirradiated and the two irradiated T91 specimens.

Similar to the SANS results, at $Q > 1\ nm^{-1}$ an irradiation effect was found, but the irradiation-induced changes are relatively smaller than in the SANS experiment. Fig. 5 compares the SANS and the SAXS patterns (measured at an X-ray energy of 5988 eV). The SANS intensity of specimen I01a was normalized to the low Q part of the SAXS patterns. This comparison suggests that the scattering contrast of the radiation defects are smaller for X-rays than for neutrons, compared with the scattering contrast of the mean inhomogeneities visible in the unirradiated state. Fig. 5 furthermore demonstrates that the irradiation induced SAXS intensity increases with irradiation temperature.

The general dependence of the SAXS intensity on the applied X-ray energy is similar for all three investigated specimens. As an example Fig. 6 shows this dependence for the raw SAXS data measured from specimen I12. At $Q > 0.4\ nm^{-1}$ the intensity

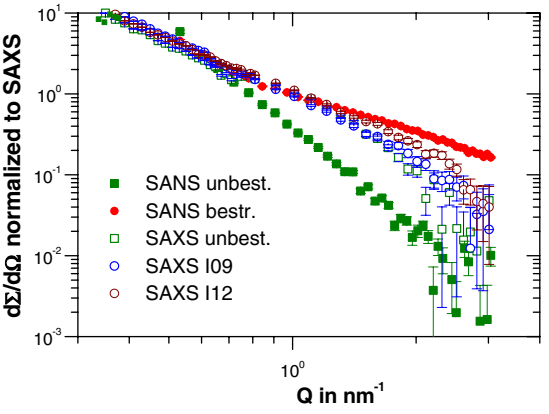

Fig. 5. Comparison of the high Q range of the SANS and SAXS curves.

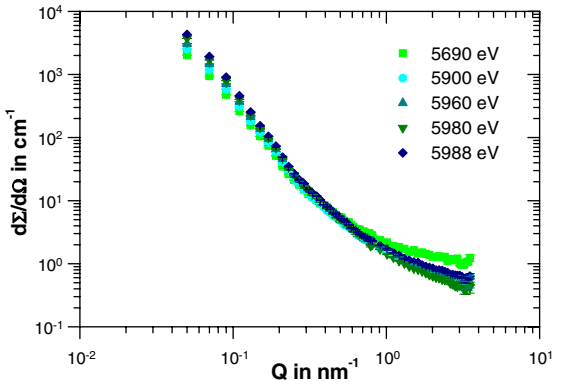

Fig. 6. SAXS patterns of specimen I12 for the different X-ray energies.

decreases with energy up to 5980 eV, then increases at 5988 eV. The strongest decrease is between 5690 and 5900 eV. In the whole Q-range the SAXS intensity of the unirradiated state is lower than the intensities of the two irradiated states. In order to analyse the intensity variation, the intensities measured at 5690 and 5980 eV were compared. Fig. 7 gives the difference of the intensities measured at 5690 and 5980 eV (I(5690 eV) − I(5980 eV)) for specimen I12 at higher Q-values. The behaviour for the other specimens is similar. It is found that the intensity difference does not depend on Q. It implies that it is not from small angle scattering, rather from fluorescence radiation of vanadium. At 5988 eV the induction of Cr fluorescence radiation begins. This intensity is proportional to the specific absorption coefficient μ/ρ of vanadium which decreases from 537.2 cm^2 at 5690 eV to 471.8 cm^2 at 5980 eV. The constant scattering contribution was determined by a Porod analysis and subtracted from the SAXS data for all measurements (see Fig. 4).

At $Q < 0.4$ nm^{-1} the scattering intensity increases with increasing X-ray energy (decreasing difference to the Cr-absorption edge). It shows that the Cr containing inhomogeneities have a smaller scattering density than the steel matrix.

As Table 3 shows the intensity difference I(5988 eV) − I(5690 eV) is nearly exclusively caused by Cr containing inhomogeneities because only f' of Cr varies significantly. In the following this intensity difference will be called the Cr effect. In Fig. 8 the Cr effect is given for the three investigated states. In the whole available Q range the Cr effect determined for the unirradiated state is lower than the effect found for the two irradiated specimens. In Fig. 9 the Cr effect of the unirradiated state is subtracted from the Cr effect found for the two irradiated specimens. It represents the SAXS patterns of the Cr rich inhomogeneities formed by the irradiation

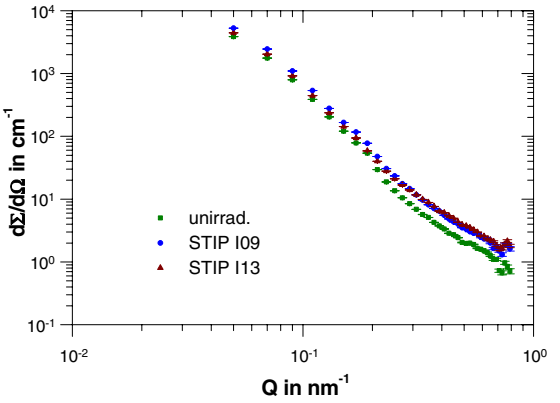

Fig. 8. Cr effect (intensity difference $I(E = 5988$ eV) − I(5690 eV)) for the measured specimens.

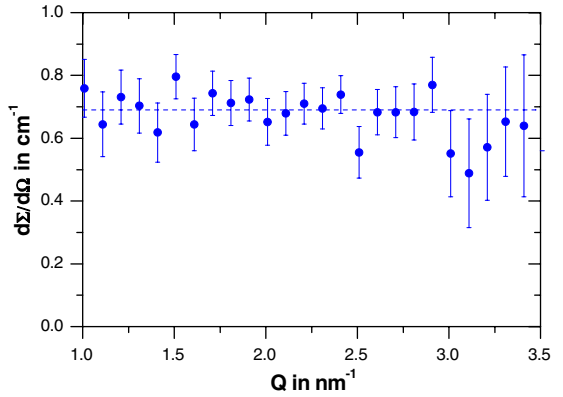

Fig. 7. Difference of intensities measured at 5690 and 5980 eV for specimen I12.

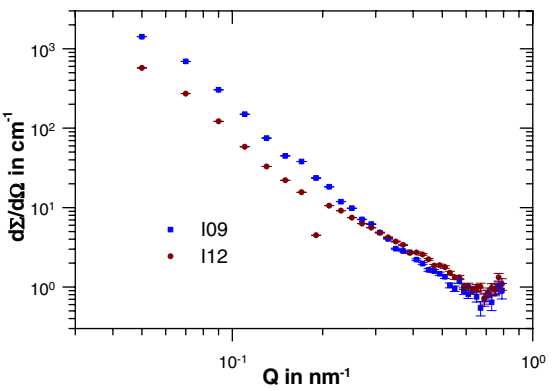

Fig. 9. SAXS patterns of the Cr containing radiation defects of sample I09 and I12.

(irradiation-induced Cr effect). The irradiation-induced Cr effect of specimen I09 shows Q dependence close to a power law with an exponent of about -3.4. From this fact it can be concluded that the Cr containing particles are larger than about 40 nm. The exponent of -3.4 is typical for volume fractals. It gives a hint that the Cr containing objects have not a well defined interface to the steel matrix. They can be for instance grain boundary segregations.

The curve for specimen I12 differs significantly from the curve determined for I09 at Q values $<0.3\ \mathrm{nm}^{-1}$. Also smaller Cr containing inhomogeneities seem to be formed. However, for this specimen the power law scattering dominates, too.

At large Q ($>0.7\ \mathrm{nm}^{-1}$) where in the SANS experiment the irradiation-induced scattering were found, no additional scattering of the Cr-rich inhomogeneities are detected. It indicates that the irradiation defects detected by SANS are not Cr-rich inhomogeneities.

Other types of radiation defects like He bubbles have to be taken into account. Due to the fact that the number density of He in the bubbles are not known, the scattering contrast relations between the bubbles and the matrix for magnetic and nuclear SANS and for SAXS cannot be calculated.

4. Conclusions

Both SANS and SAXS measurements provide information about radiation defects in T91.

In the SANS experiment strong effect of irradiation was found. The volume fraction and size of the radiation defects detected by SANS does not depend on the fluence. This may suggest a saturation of the radiation damages under these conditions.

The ASAXS investigations indicate that Cr containing inhomogeneities are formed. They are relatively large and can be grain boundary segregations. The radiation defects detected by SANS are not Cr-rich.

References

[1] M.H. Mathon, Y. de Carlan, G. Geoffroy, X. Averty, A. Alamo, C.H. de Novion, J. Nucl. Mater. 312 (2003) 236.
[2] J. Boutard, Y. Dai, K. Ehrlich, Structural Materials – Irradiation Effects and Selection, Megapie Meeting, Cadarache, 2000.
[3] X. Jia, Y. Dai, M. Victoria, J. Nucl. Mater. 305 (2002) 1.
[4] R. Coppola, M. Magnani, R. May, A. Moeslang, Appl. Cryst. 33 (2000) 469.
[5] M. Grosse, V. Denner, J. Böhmert, M.H. Mathon, J. Nucl. Mater. 277 (2000) 280.